Sensitivity Test for Benchmark Analysis of EBR-II SHRT-17 using MARS-LMR

Chiwoong Choi [a*] and Kwiseok Ha [a]
[a]*Korea Atomic Energy Research Institute, 989-111, Daedeok-daero, Yuseong-gu, Daejeon, 305-353, Korea*
[*]*Corresponding author: cwchoi@kaeri.re.kr*

1. Introduction

This study was conducted as a part of the IAEA Coordinated Research Project (CRP), "Benchmark Analyses of an EBR-II Shutdown Heat Removal Test (SHRT)" [1]. EBR-II SHRT 17 (Loss of flow) was analyzed with MARS-LMR, which is a safety analysis code for a Prototype GEN-IV Sodium-cooled Fast Reactor (PGSFR) has developed in KAERI. The current stage of the CRP is comparing blind test results with opened experimental data. Some influential parameters are selected for the sensitivity test of the EBR-II SHRT-17. The major goal of this study is to understand the behaviors of physical parameters and to make the modeling strategy for better estimation.

2. Benchmark Analysis of EBR-II SHRT-17

2.1 Physical Conditions of SHRT-17

An EBR-II SHRT-17 is a protected loss of a flow test, which was conducted where a loss of electrical power to all plant sodium coolant pumps was used to demonstrate the effectiveness of the natural circulation cooling characteristics. Fig. 1 shows the benchmark model of EBR-II [2]. The benchmark calculation domain is limited to IHX, thus the boundary conditions are applied at the IHX tube side with temperatures and mass flow rates. A sodium flow is driven by two pumps in a cold pool and divided into high (310, 340) and low (330, 360) pressure (HP and LP) pipes, which are connected to two high (370) / low (380) - pressure inlet

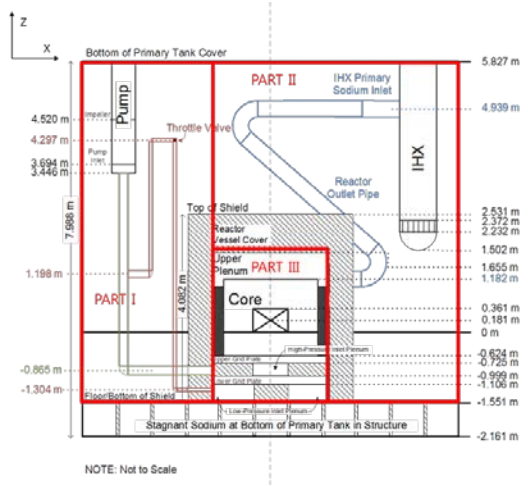

Fig. 1 Benchmark Model of Computational Domain [2]

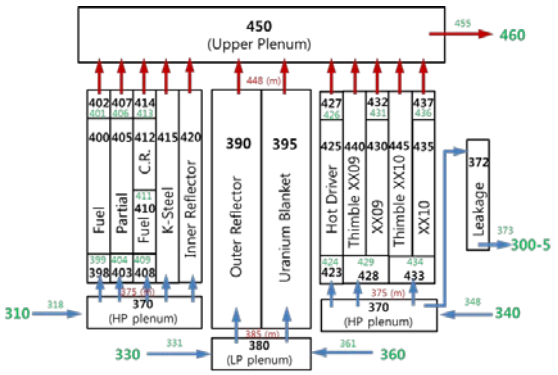

Fig. 2 Nodalizations of core region (Part III in Fig.1)

plenums, respectively. Fig. 2 shows nodalizations of the core region. 12 core subassembly (SA) groups connected between upper plenum (450) and two lower plenums are modeled. In addition, a Z-shaped pipe (460) is connected to the inlet of the IHX shell-side, and thus there is no hot pool. The IHX tube-side is modeled with inlet and outlet boundaries. A pump coastdown and power transient are also supplied as the boundary conditions. The power and flow distribution are applied with data provided by the neutronic analysis team in Argonne National Laboratory [2].

2.2 Blind Test Results

Fig. 3 shows pump flow evaluated by the MARS-LMR and SHRT-17 experimental results. Because the coast-down curve is boundary condition, the MARS-LMR shows good agreement in the initial region. However, in the natural circulation region, the pump flow was over-estimated, which means the pressure drop in the natural circulation region is under-estimated. Fig. 4 shows the temperatures in the inlets of the HP and LP inlet plenum and the Z-pipe, which indicates the temperature difference between the core inlet and outlet. The inlet temperatures of HP and LP are precisely calculated. However, the Z-pipe inlet temperature is slightly under-estimated than experimental data. One of the reasons for the lower the outlet temperature can be higher flow rate as shown in Fig. 3. Fig.5 shows temperatures in the IHX shell-side inlet and tube-side outlet, MARS-LMR shows under-estimated and over-estimated temperatures for short and long terms, respectively. These parameters were poorly estimated by all participants in this CRP as shown in Fig. 6.

EBR-II has two experimental subassemblies, the XX09 for a fueled SA, and the XX10 for a non-fueled SA. In this study, we focused on behaviors in the XX09. The XX09 SA has radial and axial measurement points as shown in Fig. 7. The TTCs are located axially and radially center. Fig. 8 shows the TTC temperatures as representative results for the XX09. The modeling of XX09 SA is treated a radially averaged single volume. Therefore, it is impossible to directly compare temperature evaluated by the MARS-LMR and that locally measured the thermocouples.

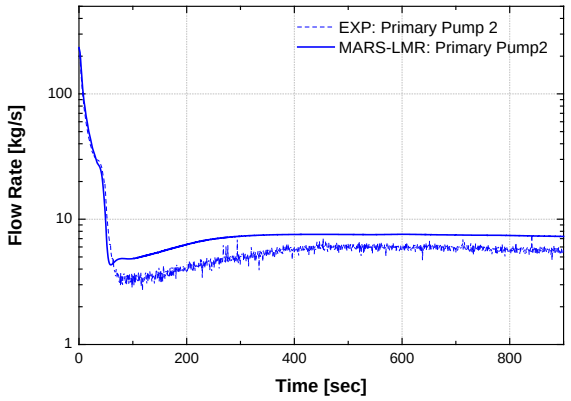

Fig. 3 Primary pump flow rate during SHRT-17

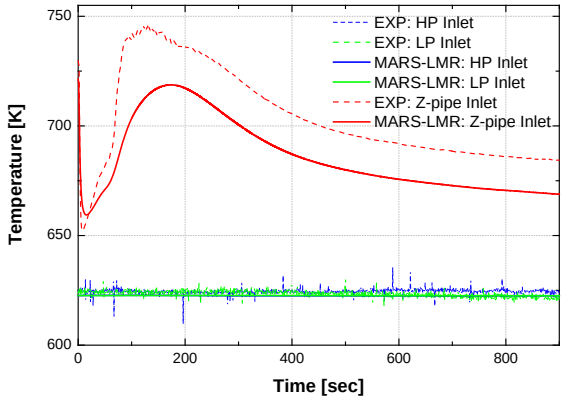

Fig. 4 Inlet temperatures of the HP and LP inlet plenum and the Z-pipe during SHRT-17

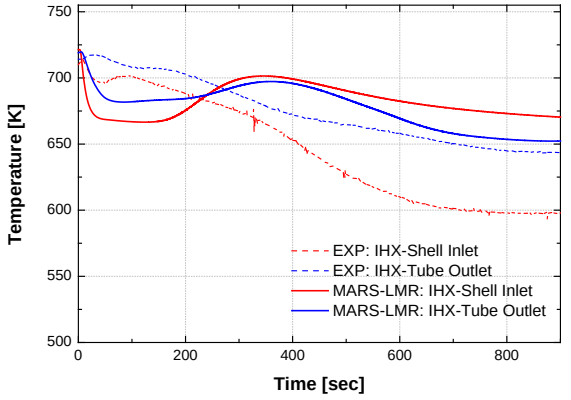

Fig. 5 Temperatures in IHX shell-side inlet and tube-side outlet during SHRT-17

The temperature from the MAR-LMR is a mean temperature of radial distribution. So, it should be mean temperatures among the measured temperature. The measured radial temperatures had distribution with approximately 40 K. And the MARS-LMR estimated the lowest temperature in Fig. 8.

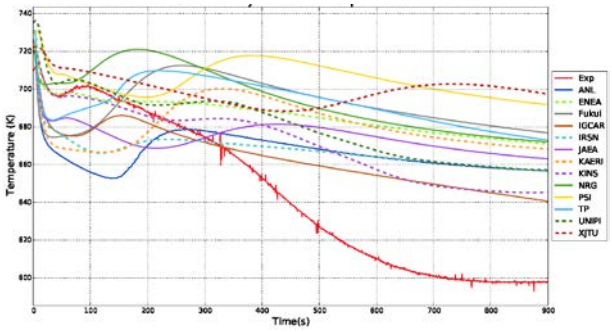

Fig. 6 All participants results for the IHX shell-side inlet temperature during SHRT-17

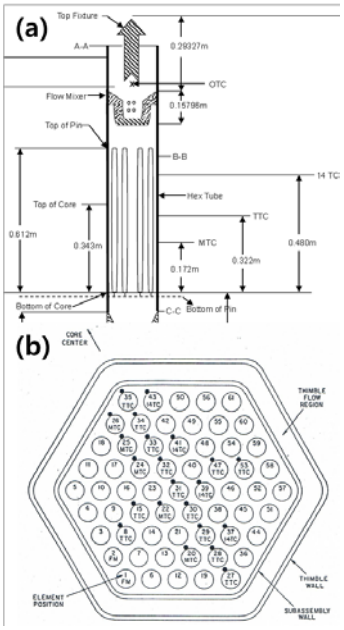

Fig. 7 Cross sectional view of XX09: (a) axial, and (b) radial

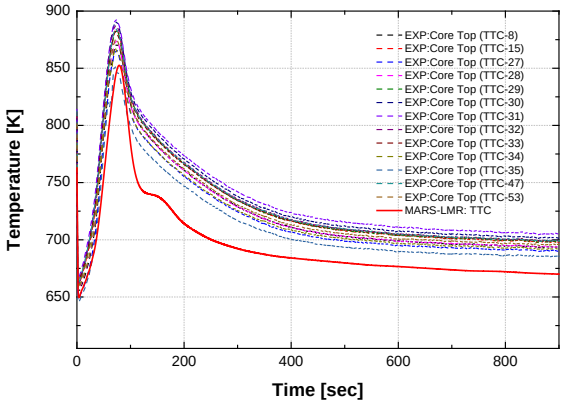

Fig. 8 Temperature at TTC in the XX09 during SHRT-17

3. Sensitivity Test

3.1 Parameters for Sensitivity Test

Flow and power distribution during a transient is most important parameter, because temperatures in each subassembly are ruled by a power to flow ratio. In addition, in natural circulation region, a temperature difference drives flow, which means fluid temperatures coupled with flow. As discussed in the blind test results, the most critical parameter in the SHRT-17 was flow rate in the natural circulation region. However, it is very difficult to correct without the pressure drop information under the low flow rate. It will be considered after requesting the related data to ANL. As shown in Fig. 7, the experimental SAs have a bundle region as inner part and a thimble region of another hexagonal duct, which has a flow and heat transfer from the bundle to the thimble region. The thimble part is also modeled as shown in Fig. 9. The flow rate in the XX09 thimble region and the heat transfer rate from the duct wall to the thimble region are important but unknown. Thus, those parameters are selected as sensitivity test parameters.

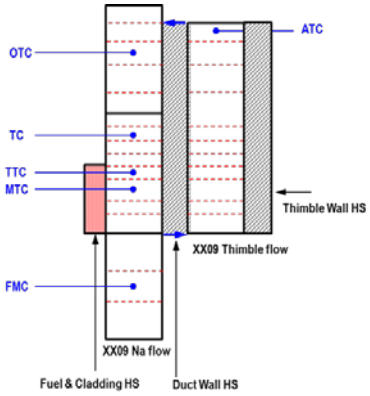

Fig. 9 Modeling of XX09 SA with thimble region

3.2 Total Power in XX09

Power portion in the XX09 are increased to 50%. As increasing the power portion in the XX09, obviously, the temperature is increased and the peak temperature is shown earlier. The peak temperature is reached to the maximum measured value. The flow rate in the XX09 is increased as the power portion in the XX09 is increased as shown in Fig. 11. The reason is that the temperature rise induces buoyant force and it increases flow rate. The power change in the XX09 has no influence on the rest of variables.

3.3 Initial Total Flow in XX09

Initial flow rate in the XX09 are reduced to 75%. Fig. 12 shows the sensitivity of the flow rate in the XX09. As decreasing the flow rate in the XX09, obviously, the temperature is increased and the peak temperature slightly delayed. The peak temperature is reached to middle between the maximum and the minimum temperatures. And the flow rate in the XX09 is decreased as the initial flow rate increased as shown Fig. 13. In addition, the flow rate in the natural circulation region is highly affected than the transition region by the initial flow rate change comparing the effect of the power change. The initial total flow rate in the XX09 has no influence on the rest of variables.

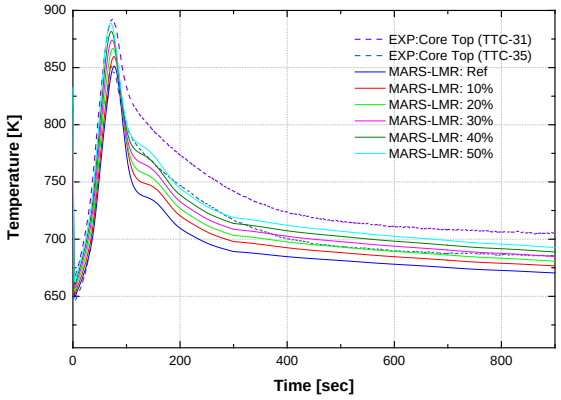

Fig. 10 TTC temperatures for different power in the XX09 during SHRT-17

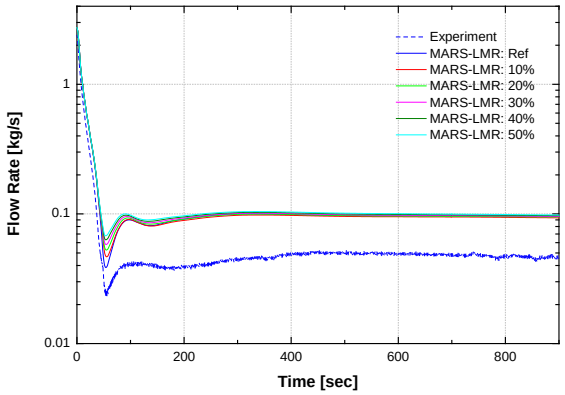

Fig. 11 Flow rate in the XX09 for different power in the XX09 during SHRT-17

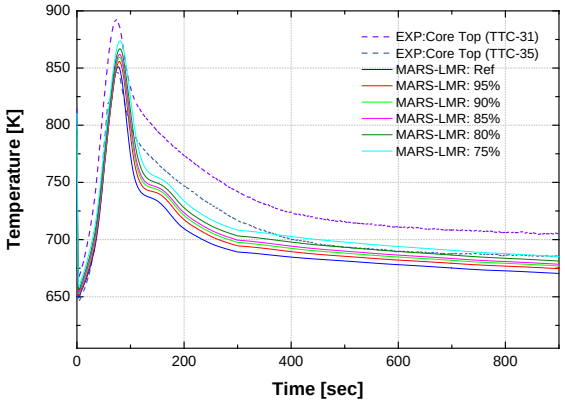

Fig. 12 TTC temperatures for different initial flow rate in the XX09 during SHRT-17

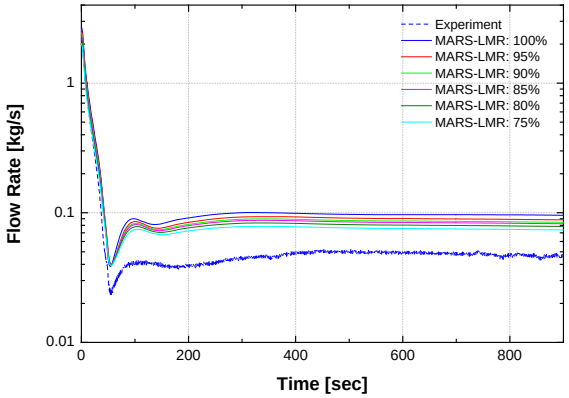

Fig. 13 Flow rate in the XX09 for different initial flow rate in the XX09 during SHRT-17

3.2 Thimble Flow in XX09

A flow in the XX09 is separated to the bundle and the thimble regions. If the flow rate in the thimble region is increased, the TTC temperatures will be increased due to reduction of flow in the bundle region. The thimble flow in the reference case is about 11% of total flow in the XX09. So, the thimble flow rate is increased to 48%. Fig. 14 shows TTC temperature for different flow

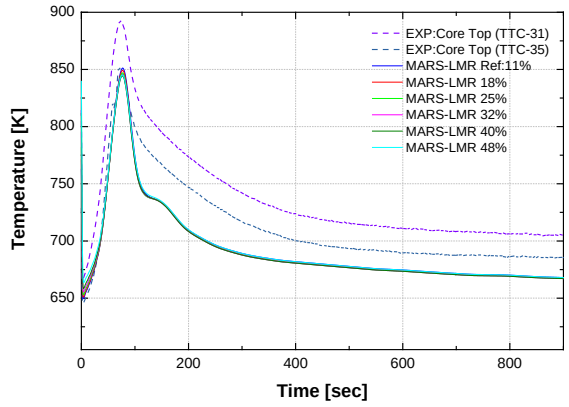

Fig. 14 TTC Temperatures for different thimble flow rates

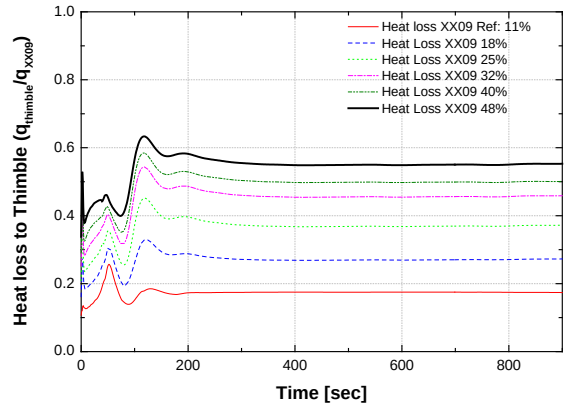

Fig. 15 Heat loss to the thimble region for different initial thimble flow

portion in the thimble region, which shows the coolant temperature was not sensitive to the thimble flow change. Even though the flow rate in the bundle region is decreased, the heat loss to the thimble region is also increased as shown in Fig. 15, due to increased flow rate in the thimble region. In addition, the initial flow rate has no influence on the rest of variables.

3.5 Thimble Wall Heat Transfer in XX09

The heat loss from the bundle to the thimble region is governed by heat transfer through the duct wall, which has no appropriate correlation. The modified Shad's [3] and Aoki's [4] correlations are supplemented in the MARS-LMR for the bundle side and tube side, respectively. In this study, the heat transfer rate is changed from 100% to 3.125%. Fig. 16 shows ATC temperatures, which is located at the outlet of the thimble region as described in Fig. 9. The reference case shows higher temperature than the experimental data, which means the heat loss is over-estimated in calculation. Fig. 17 shows TTC temperatures for different heat transfer rate from the bundle to the thimble region. Basically, as reducing the heat loss to the thimble region, the TTC temperatures must be increased. However, these results represent opposite way. As reducing the heat loss to the thimble

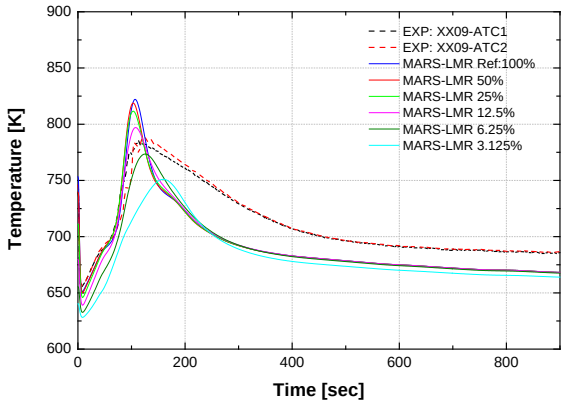

Fig. 16 ATC temperatures for different heat loss ratio

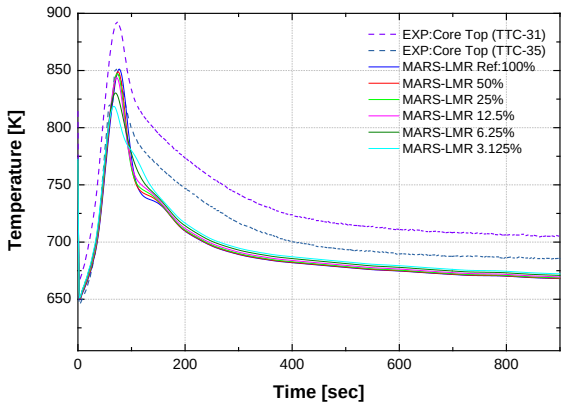

Fig. 17 TTC Temperature for different heat loss ratio

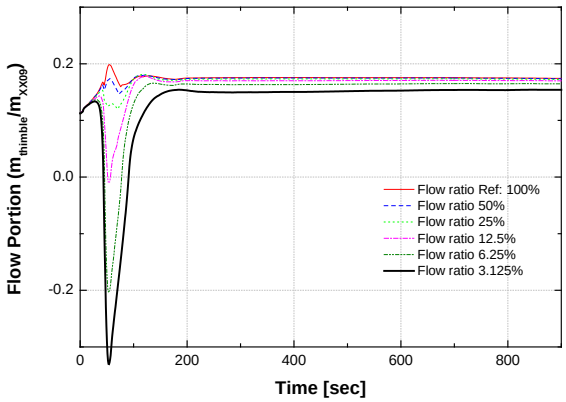

Fig. 18 Thimble Flow portion for different heat loss ratio

region, the flow rate in the thimble region also reduced due to reduction of buoyancy force as shown in Fig. 18. In addition, for cases of the lower heat transfer rate than 12.5 %, flow reversals occurred. The flow portion in the bundle region is increased, and the TTC temperatures are decreased. These results indicate that the flow distribution is highly related to thermal characteristics in the subassemblies.

3. Discussion

The Korea Atomic Energy Research Institute (KAERI) has designed a Gen-IV prototype sodium cooled fast reactor (PGSFR). The safety analysis of the PGSFR has been conducted using the MARS-LMR code, which is a liquid metal version of the MARS code. To validate and evaluate the MARS-LMR code, we joined the EBR-II benchmark analysis of IAEA CRP. EBR-II SHRT-17 was analyzed using MARS-LMR with input data supplied by Argonne National Laboratory (ANL).

The overall results of MARS-LMR for the SHRT-17 indicate similar tendencies with experiments except the core outlet temperatures. Totally, the primary flow is over-estimated, thus most of temperatures are under-estimated. In this study, we conducted sensitivity tests for some parameters. The experimental subassemblies, XX09 and XX10 in the EBR-II, have a thimble region, in which the flow rate and heat loss are unclear. So, the flow rate and the heat transfer rate in the thimble region are also considered as sensitivity test parameters. The thimble flow rate and heat transfer through the thimble wall are highly related to each other. The convective heat transfer in the thimble region is governed by the flow rate, and the higher heat transfer rate generates a higher buoyancy force, which affects the flow resistance working as the key parameter in the flow distribution.

For the next step, the primary flow rate will be matched using sensitivity test for the primary side flow resistance, which will be intensive works because there is no pressure loss information during the natural circulation condition. In addition, the core outlet temperature will be focused with appropriate parameters, for example, leakages to a pool side or Z-pipe heat structure. The current sensitivity results can be used for fine modification for future benchmark analysis of SHRT-17 and additional EBR-II SHRT cases.

REFERENCES

[1] L. Briggs et al., “Benchmark Analyses of the Shutdown Heat Removal Tests Performed in the EBR-II Reactor,” FR13, Paris, France, March 4-7 (2013).
[2] T. Sumner and T. Y. C. Wei, “Benchmark Specification and Data Requirements for EBR-II Shutdown Heat Removal Test SHRT-17 and SHRT-45R, ANL-ARC-226 (Rev.1), (2012).
[3] M. S. Kazimi and M. D., “Heat Transfer Correlation for Analysis of CRBRP Assemblies,” Westinghouse Report, CRBRPARD-0034, (1976)
[4] S. Aoki, “Current Liquid-metal Heat Transfer Research in Japan,” Prog. Heat Mass Transfer, Vol. 7, (1973)